HHS Public Access

Author manuscript

Osteoarthritis Cartilage. Author manuscript; available in PMC 2018 January 01.

Published in final edited form as:

Osteoarthritis Cartilage. 2017 January ; 25(1): 108–117. doi:10.1016/j.joca.2016.08.008.

Nanoindentation Modulus of Murine Cartilage: A Sensitive Indicator of the Initiation and Progression of Post-Traumatic Osteoarthritis

Basak Doyran[1,a], **Wei Tong**[2,3,a], **Qing Li**[1], **Haoruo Jia**[2], **Xianrong Zhang**[4], **Chider Chen**[5], **Motomi Enomoto-Iwamoto**[6], **X. Lucas Lu**[7], **Ling Qin**[2,*], and **Lin Han**[1,*]

[1]School of Biomedical Engineering, Science, and Health Systems, Drexel University, Philadelphia, PA 19104, United States

[2]Department of Orthopaedic Surgery, Perelman School of Medicine, University of Pennsylvania, Philadelphia, PA 19104, United States

[3]Department of Orthopaedic Surgery, Union Hospital, Tongji Medical College, Huazhong University of Science and Technology, Wuhan, 430022 Hubei, China

[4]Department of Physiology, School of Basic Medical Sciences, Wuhan University, Wuhan, Hubei 430071, P. R. China

[5]Department of Anatomy and Cell Biology, School of Dental Medicine, University of Pennsylvania, Philadelphia, PA 19104, United States

[6]Department of Surgery, The Children's Hospital of Philadelphia, Philadelphia, PA 19104, United States

[7]Department of Mechanical Engineering, University of Delaware, Newark, DE 19716, United States

Abstract

Objective—This study aims to demonstrate that cartilage nanoindentation modulus is a highly sensitive indicator of the onset and spatiotemporal progression of post-traumatic osteoarthritis (PTOA) in murine models.

[*]Correspondence and requests for materials should be addressed to: Dr. Lin Han, Phone: (215)571-3821, Fax: (215)895-4983, lh535@drexel.edu. Dr. Ling Qin, Phone: (215)573-2133, Fax: (215)898-3261, qinling@mail.med.upenn.edu.
[a]B. Doyran and W. Tong contributed equally to this work.

Conflict of Interest The authors of this study have no personal or financial conflicts of interest with this work.

Contributions

BD and WT contributed to the concept and design of the study, including data collection, analysis and interpretation, as well as drafting and revising of the manuscript. QL, HJ, XZ, CC and ME-I contributed to the collection and interpretation of experimental data. LH, LQ, and XLL contributed to the concept and design of the study, including obtaining of funding, interpretation of the data, and writing and critical revision of the article for intellectual content. All authors approved the final version of the article. First (BD, WT) and last (LH, LQ) authors take responsibility for the integrity of the work as a whole, from inception to finished article.

Design—Destabilization of medial meniscus (DMM) surgery was performed on the right knees of 12-week old male, wild-type C57BL/6 mice, with Sham control on contralateral left knees. Atomic force microscopy (AFM)-based nanoindentation was applied to quantify the nanoindentation modulus, E_{ind}, of femoral condyle cartilage at 3 days to 12 weeks after surgery. The modulus changes were compared against the timeline of histological OA signs. Meanwhile, at 8 weeks after surgery, changes in meniscus, synovium and subchondral bone were evaluated to reveal the spatial progression of PTOA.

Results—The modulus of medial condyle cartilage was significantly reduced at 1 week after DMM, preceding the histological OA signs, which only become detectable at 4 – 8 weeks after. This reduction is likely due to concomitantly elevated proteolytic activities, as blocking enzymatic activities in mice can attenuate this modulus reduction. In later OA, lateral condyle cartilage and medial meniscus also started to be weakened, illustrating the whole-organ nature of PTOA.

Conclusions—This study underscores the high sensitivity of nanoindentation in examining the initiation, attenuation and progression of PTOA in murine model. Meanwhile, modulus changes highlight concomitant changes in lateral cartilage and meniscus during the advancement of OA.

Keywords

post-traumatic osteoarthritis; nanoindentation; cartilage; destabilization of the medial meniscus (DMM); murine models

INTRODUCTION

Post-traumatic osteoarthritis (PTOA) is a prevalent form of OA in young adults, characterized by injury-induced irreversible breakdown of articular cartilage and other synovial tissues.[1] It originates either from direct injury of cartilage surfaces, joint fractures, or from load instabilities created by ligamentous or meniscal damages.[2] Contrary to the aging-induced spontaneous OA, PTOA tends to affect younger and active adults, leading to a lengthier duration of disability and a higher financial burden.[3] In addition, PTOA takes a molecular pathology distinctive from the spontaneous OA.[4] Currently, molecular etiology and functional symptoms of PTOA are not well-defined, and thus, the search of predictive biomarkers and the development of effective therapeutics are still at the early stage.[5,6]

Murine models offer a unique stepping stone to bridge basic orthopaedic research with clinical practices of OA treatments,[7] whereby genetic modifications are used in combination with surgical or other induced forms of OA.[8] In these studies, the degree of OA in mice is normally defined by tissue-level symptoms measured via histology[9] and microcomputed topography (μCT).[10] Semi-quantitative scoring systems, such as the Mankin and OARSI scores,[9] are used to describe micro-to-macroscopic structural and compositional changes. These assays, however, cannot detect PTOA until irreversible, tissue-level cartilage damage has taken place, nor can they directly show compromises in the primary biomechanical functions of cartilage, such as load bearing and shock absorption. The study of disease-related changes in tissue biomechanical properties can, however, address both issues. First, mechanical properties are direct indicators of cartilage function. Second, mechanical changes represent integrated responses of compositional and structural alterations.[11] Third,

if mechanical changes can be measured at smaller scales, e.g., deformation with contact lengths on the order of 1 μm or less (known as “nanomechanical symptoms”), they may precede macroscopic changes, aiding earlier detection of OA.

The objective of this study is to reveal the nanomechanical symptoms of articular cartilage in murine PTOA, and to demonstrate its potential in serving as a sensitive indicator of OA initiation, attenuation and progression. PTOA will be induced in wild-type mice via the destabilization of the medial meniscus (DMM) surgery.[12] The DMM model is a well-defined joint instability-induced OA model, and has been widely used to study the roles of various molecular signaling pathways in PTOA.[13–17] After DMM, mild-to-moderate histological OA signs usually start at 4 weeks, and become significant at 8–12 weeks.[12] To evaluate the chronological changes in the nanomechanical properties of cartilage, we performed atomic force microscopy (AFM)-based nanoindentation on femoral condyle cartilage surfaces from 3 days to 12 weeks after DMM, and compared the results against joint morphological changes detected by histology and μCT. To reveal the spatiotemporal progression of OA, we compared the mechanical changes of condyle cartilage and meniscus on both the medial and lateral sides at 8 weeks post-surgery. To test the sensitivity of nanoindentation in evaluating PTOA attenuation, we blocked catabolic enzymatic activities by GM6001 injection immediately after DMM, and examined whether this treatment can alleviate cartilage weakening at one week post-surgery.

METHODS

Animal surgery

Skeletally mature, 12-week old male C57BL/6 wild-type mice (The Jackson Laboratory, Bar Harbor, ME) were subjected to the DMM and Sham surgeries on the right and left knees, respectively, following established procedures.[16] Only male mice were used because they develop more severe OA than females after DMM.[18] Under DMM, immediately after anesthesia, the right knee joint capsule was opened and the medial meniscotibial ligament was cut to destabilize the medial meniscus without damaging other tissues. Under Sham, the left joint capsule was opened in the same fashion to expose the ligament but without any further damage. Mice were maintained in their preoperative groups, allowed unrestricted cage exercise, and were weighted weekly until they were euthanized. All animal work performed in this study was approved by the Institutional Animal Care and Use Committee (IACUC) at the University of Pennsylvania.

Atomic force microscopy (AFM)-based nanoindentation

After euthanasia, bilateral distal femurs were dissected free of tendon and ligament tissues and glued onto AFM sample discs by a cyanoacrylate adhesive gel (Loctite 409, Henkel Corp., Rocky Hill, CT), as described previously.[19] Throughout the procedure, femurs were maintained in PBS with protease inhibitors (Pierce 88266, Fisher Scientific, Rockford, IL) to minimize post-mortem degradation. AFM-based nanoindentation was performed on the surfaces of femoral condyle cartilage using a borosilicate colloidal spherical tip ($R \approx 5$ μm, nominal $k \approx 7.4$ N/m, AIO-TL, cantilever C, NanoAndMore, Lady’s Island, SC) and a Dimension Icon AFM (BrukerNano, Santa Barbara, CA) (Fig. 1a,b). For each condyle

cartilage at each time point (n = 5–12), at least 10–15 different indentation locations were tested on the load bearing regions at 1 to 10 μm/s AFM z-piezo displacement rates (approximate indentation rates). At each location and rate, nanoindentation was repeated for three times, with 2–3 seconds dwell time between each repeat, and the F-D curves are highly consistent amongst the three repeats. Each indentation was performed up to a maximum indentation force ≈ 1 μN, corresponding to a maximum indentation depth ≈ 0.4–1 μm (e.g., D_{max} = 0.36 [0.29 0.43] μm for Sham, 1.14 [0.90 1.38] μm for DMM on medial condyles at 8 weeks post-surgery, mean [95% CI], n = 10).

The effective indentation modulus, E_{ind}, was calculated by fitting the entire loading portion of each F-D curve to the Hertz model (Fig. 1c),

$$F=\frac{4}{3}\frac{E_{ind}}{(1-\nu^2)}R^{1/2}D^{3/2}.$$

where R is the tip radius, and ν is the Poisson's ratio (≈ 0.1 for cartilage[20]). Here, we did not apply the Oliver-Pharr method to the unloading curve, since the Oliver-Pharr method assumes elastic-plastic material deformation,[21] a distinctive mode from the reversible poroviscoelastic deformation of cartilage.[22] Under poroviscoelastic relaxation, calculation of elastic recovery modulus based on the unloading F-D curve slope can lead to falsified high $E_{O\text{-}P}$ values, whereas such artifact is absent when applying the Hertz model to the loading F-D curve. While the Hertz model does not capture the time-dependent, poroviscoelastic characteristics of cartilage, it provides a direct measure of cartilage's "effective indentation modulus" at a given rate.[23] Comparing the modulus measured at the same rate amongst different conditions, such as Sham versus DMM, can therefore identify relative differences in their mechanical behaviors. In addition, following the same procedure,[24] nanoindentation was performed on the non-ossified, central region, proximal surfaces of medial and lateral menisci at 8 weeks after surgery (n = 5).

Histology and immunohistochemistry

For histology, additional mice were euthanized at 4–12 weeks after surgery (n = 5/time point). Whole joints of both knees were harvested, fixed in 4% paraformaldehyde, decalcified in 10% EDTA, and embedded in paraffin. Serial 6-μm-thick sagittal sections were cut across the joint and two sections within every consecutive six sections were stained with Safranin-O/Fast Green. From each knee, approximately 15 sections were obtained and scored by at least two blinded observers (WT and HJ) using the modified Mankin method.[9] To quantify the loss of articular cartilage, cartilage area (total) and Safranin O-stained area (uncalcified) were outlined and their thicknesses were determined by averaging 5 thickness values evenly distributed across the entire cartilage. To detect the inflammation of synovium, for each knee, the paraffin section near the one with maximal Mankin score was stained with hematoxylin and eosin (H&E) to examine the increase in the synovial lining cellular layers at the edge of synovium, the increase in cell density throughout the whole synovium membrane and the presence of inflammatory cells.[25] To detect matrix degradation products in articular cartilage, paraffin sections from mice at 2 weeks after surgery were processed for

immunohistochemical (IHC) staining of aggrecan degradation neoepitopes by matrix metalloproteinases (MMPs) (VDIPEN[341],[26] a gift from Dr. John S. Mort), as described previously.[27]

Micro-computed tomography (μCT) analysis

To reveal the concurrent changes of subchondral trabecular bone, bilateral femurs were harvested from additional mice ($n = 10$) at 8 weeks post-surgery for *ex vivo* μCT analyses (microCT 35, Scanco Medical AG, Brüttisellen, Switzerland). The distal end of the femur corresponding to a 0–4.1 mm region was scanned at 6 μm isotropic voxel size to acquire 686 μCT slices per scan. All images were smoothed by a Gaussian filter (sigma = 1.2, support = 2.0) and contoured at a threshold corresponding to 30% of the maximum available range of image gray scale. To quantitatively describe the subchondral bone morphology and properties, bone volume fraction (BV/TV), structure model index (SMI), trabecular number (Tb.N), trabecular thickness (Tb.Th) and trabecular separation (Tb.Sp) were calculated by 3D standard microstructural analysis provided by the manufacturer.

Fluorescence imaging and blocking of catabolic enzymatic activities

To detect the proteolytic cleavage of aggrecan by catabolic enzymes, such as MMPs, MMPSense™ 645 FAST (100 μL/mouse) was injected by tail vein into additional mice ($n = 5$) at 6 days after surgery. Although optically silent upon injection, this agent can produce fluorescent signal after cleavage by disease related activation of various MMPs.[28] To perform ex vivo imaging, femurs and tibiae were harvested at day 7 and immediately placed on the black plates for image acquiring at 649 nm excitation and 666 nm emission wavelengths. The fluorescence intensities, total radiant efficiency [p/s/cm^2/sr]/[μW], on cartilage were analyzed by Living Image 4.2 (Perkin Elmer).

To determine whether elevated catabolic enzyme activities are a major cause of the early cartilage mechanical weakening after DMM, additional mice ($n = 5$) were intraperitoneally injected with 4 mg/kg/day GM6001 (sc-203979, Santa Cruz Biotech., Dallas, TX) daily starting from one day before surgery, and were sacrificed at 1 week after surgery for AFM-based nanoindentation tests. GM6001, a hydroxamate zinc-chelating active site-directed enzyme inhibitor, can effectively block MMP activities, and largely reduce aggrecanase activities.[29] For the control group ($n = 10$), same amount of vehicle dimethyl sulfoxide (DMSO) was injected subcutaneously starting from one day before surgery.

Statistical tests

Kolmogorov-Smirnov test suggested that the data distribution is significantly different from normal, and thus, non-parametric tests were used. For each time point and surgery type, the observed distribution of E_{ind} (e.g., Fig. 1d) can be originated from animal-to-animal variations, structural heterogeneity of cartilage surface within each joint, and spatial heterogeneity in cartilage degradation during PTOA. In this study, significance in the differences between the DMM and Sham knees hinges on the consistency of modulus reduction in multiple animals. Therefore, instead of pooling modulus values of all locations from different animals, we first calculated the average values of E_{ind} from multiple locations of each condyle, and then, performed statistical tests on these average values from different

animals for each time point and surgery type. Since DMM and Sham surgeries were performed on the same mouse, Wilcoxon signed rank test[30] was used to compare the values of E_{ind}, Mankin score, t_{total}, $t_{uncalcified}$, μCT outcomes, synovium OA grades, and MMP activities at each time point. To study the impacts of mechanical heterogeneity on the significance within each animal, Mann-Whitney U rank sum test was performed on E_{ind} at different locations measured on the DMM versus Sham joint. In all the tests, a p-value < 0.05 was considered statistically significant.

RESULTS

Histological OA signs

Histology detected salient cartilage morphological changes after DMM. On the medial side, the signs of OA were not significant in either femoral condyle or tibial plateau of DMM knees at 4 weeks post-injury (Fig. 2a,b), consistent with other DMM studies.[12] The signs became evident, including cartilage surface fibrillation, proteoglycan staining reduction and cartilage thinning, at 8 and 12 weeks after DMM, resulting in significant modified Mankin scores (Fig. 2c). Significant reduction in the thickness of uncalcified and total cartilage illustrated clear signs of cartilage erosion (Fig. 2d,e). Meanwhile, on the lateral side, we observed a marginal Mankin score of 1.50 [0.59 2.41] at 12 weeks after DMM (n = 4, mean [95% CI]). During the 12-week period, no morphological changes were detected in the contralateral Sham knees.

Reduction in cartilage nanoindentation modulus precedes histological signs

The reduction in effective nanoindentation modulus, E_{ind}, was shown to markedly precede histological signs on the medial side (Fig. 3a). At 3 days post-surgery, moduli of medial condyle cartilage were comparable between DMM and Sham knees. By contrast, at 1 week post-surgery, a much earlier time point than when histological changes become noticeable, modulus of the DMM knee was significantly reduced to 49 [41 57]% (mean [95% CI]) of the Sham control. Later on, the DMM cartilage modulus was further declined to 34 [22 46]%, 32 [24 40]%, and 20 [14 26]% of the Sham control at 2, 4, and 8 weeks post-surgery, respectively. However, at 12 weeks post-surgery, the modulus of DMM knee was markedly elevated, to a level similar of the Sham knee (82 [70 94]%). For the lateral condyle cartilage, significant modulus reduction was detected at 4 weeks after DMM, but to a lesser extent than the medial side (Fig. 3b). However, modulus reduction of lateral cartilage also markedly preceded histological changes (4 weeks versus 12 weeks after DMM). For the Sham knee cartilage, as expected, the modulus is retained in a consistent range throughout the tested time frame.

The contrast of E_{ind} between the DMM and Sham knees of each individual mouse is consistent with the overall trend. For example, for each mouse examined at 1 week post-DMM, statistical tests comparing modulus at individual locations of each animal suggested the reduction of DMM knee is significant even accounting for the spatial heterogeneity within each knee (Fig. 4a), the same conclusion as the results from Wilcoxon signed rank test performed on the average E_{ind} values of all tested animals (Fig. 3a). In addition, the modulus contrast between DMM and Sham knees were also consistent across different

indentation rates from 1 to 10 μm/s, as shown for 1 week post-surgery (Fig. 4b). Given the poroviscoelastic nature of cartilage, the difference is more pronounced at faster rate. We therefore focused the comparison on E_{ind} at the high indentation rate of 10 μm/s.

Cartilage surface weakening is associated with elevated proteolytic activities

At 2 weeks post-surgery, IHC staining detected salient aggrecan degradation VDIPEN^{341} neoepitopes by MMPs on the DMM knees, but not on the Sham knees (Fig. 5a). To detect in vivo MMP activities, we injected MMPsensor into mice at 1 week after DMM. Interestingly, the fluorescence intensity of the MMPSensor in cartilage of DMM knees were significantly stronger than that of Sham knees (Fig. 5b), indicating that catabolic enzymatic activities, such as MMPs, were elevated rapidly during OA initiation.

The MMP and aggrecanase inhibitor GM6001 effectively suppressed these enzymatic activities in vivo, as shown by the reduced MMPSensor signals (Fig. 5b). Meanwhile, this inhibitor significantly attenuated the modulus reduction on the DMM knees ($p = 0.0059$ compared to the vehicle treated DMM knees, $n = 5$, Fig. 5c), resulting in values of E_{ind} similar to the Sham control ($p = 0.080$, $n = 5$). These data clearly indicated that the reduction of E_{ind} at the early stage after DMM was due to increased proteolytic activities.

Changes in meniscus, subchondral bone and synovium at 8 weeks after DMM

At 8 weeks after DMM, AFM-nanoindentation detected that the reduction of E_{ind} was significant for the medial menisci, but only marginal for the lateral menisci (Fig. 6a). The effective moduli of the Sham knee menisci were similar to our previously reported values of age-matched, normal murine menisci.[24] By contrast, for the synovium, histology did not reveal appreciable signs of inflammation and hyperplasia, such as synovial lining thickening, increased cellularity or inflammatory cell infiltration (Fig. 6b). For the subchondral bone, μCT analysis did not show any significant changes in trabecular structure between DMM and Sham joints (Fig. 6c).

DISCUSSION

1. Nanoindentation modulus: a sensitive indicator of the early onset and attenuation of PTOA

The modulus decrease of medial condyle cartilage at 1 to 2 weeks after DMM (Fig. 3a) underscores the high sensitivity of E_{ind} to PTOA. In this study, the maximum indentation depth D_{max} is up to ≈ 0.4–1 μm. Under the spherical tips, the stress distribution extends to a depth ≈ $10\times D_{max}$,[31] values of E_{ind} therefore represent the effective indentation resistance of the top ~4–10μm cartilage layer. This layer includes the superficial zone and partly the middle zone of uncalcified hyaline cartilage (thickness ≈ 50–100μm in mice).[32] Since cartilage mechanical properties are an integrated contribution of cartilage extracellular matrix (ECM) composition and structure,[11] they can be influenced by both compositional and structural changes of the ECM at the molecular level. In fact, aggrecan fragmentation and collagen fibril disorganization in the superficial layer are characteristic molecular events of early OA.[33] Such changes can lead to the observed modulus reduction, but does not result in appreciable gross-level histological changes. Furthermore, differences of E_{ind} between

DMM and Sham cartilage increase with loading rate (Fig. 4b, 1 week after surgery), suggesting at this early stage, the molecular-level changes also alter poroviscoelastic properties of cartilage, such as viscosity and hydraulic permeability. This early compromise of superficial layer mechanical integrity can drastically reduce the fluid support capability in cartilage, increase the friction coefficient of articular surface, and initiate fast wearing.[34,35]

Our results also underscore that E_{ind} can serve as a sensitive indicator for examining the efficiency of PTOA attenuation. The early reduction of E_{ind} is due to enhanced catabolic enzymatic activities, as highlighted by both the increased MMPSense signaling at 1 week after DMM (Fig. 5b), and presence of VDIPEN[341] at 2 weeks after (Fig. 5a). These results are in agreement with the dogma that MMPs and aggrecanases are responsible for cartilage degradation in OA.[36] They also suggest a possible pivotal role of MMPs in the early onset of PTOA, similar to the dominating role of MMPs in overload-induced early aggrecan degradation in the intervertebral disc.[37] Blocking MMP and aggrecanase activities immediately after DMM can therefore attenuate such cartilage degeneration (Fig. 5c), and this therapeutic effect can be captured by nanoindentation.

2. Mechanical symptoms of medial cartilage in intermediate and late PTOA

After the early cartilage weakening up to 2 weeks post DMM, the modulus of medial condyle cartilage persists at a considerably low level from 2 to 8 weeks (≈ 20–35% of original value, Fig. 3a). During OA progression, proteoglycan content on cartilage surface could remain similar,[33] as loss in surface proteoglycan is compensated by gradual diffusion of proteoglycan fragments from the underneath middle/deep zones. Therefore, while the entire cartilage tissue is progressively degenerating, modulus of superficial zone remains at a consistent range. During this period, the reduction in modulus and increase in Mankin scores are in agreement with previous macroindentation studies of human OA cartilage, where the increase in OA scores is highly correlated with the decrease in indentation modulus.[38,39]

At 12 weeks after DMM, cartilage modulus of the DMM knee is significantly increased compared to earlier time points (Fig. 3a). One possible explanation is that when the superficial layer is eroded, as suggested by the decrease in $t_{uncalcified}$ (Fig. 2e), AFM-nanoindentation now measures the modulus of newly exposed middle/deep layers, which have higher compressive modulus than the superficial layer.[40] Other cartilage structural changes, such as exposure of calcified cartilage and growth of bone osteophytes, may also contribute to this modulus change. These data point out the limitation of using AFM-nanoindentation to detect late OA cartilage biomechanical changes. At this stage, the modulus change is not a direct indicator of the loss in cartilage mechanical stiffness. In late OA, degradation of cartilage and changes of other synovial tissues are heterogeneous and site-specific. While current study is limited to this specific time point of 12 weeks, and specific anatomical site of cartilage surface, our ongoing studies aim for further analyses of biomechanical and structural changes in those tissues at multiple late OA time points to depict the underlying mechanisms.

3. Spatiotemporal progression of PTOA

Weakening of lateral condyle cartilage starts at 4 weeks after DMM (Fig. 3b), a much later time than the directly injured medial condyle. At 12 weeks, this reduction remains moderate and Mankin scores are marginal. Since DMM directly affects the medial side loading, it is expected that lateral cartilage degradation, if present, is lesser. Here, nanoindentation results clearly illustrate the presence of progression of OA from the medial to the lateral side, highlighting the whole joint nature of OA. Such changes could be due to elevated catabolic enzymatic activities in the joint capsule, and altered lateral side cartilage contact mechanics upon the degradation of medial cartilage.[41]

At 8 weeks after DMM, in addition to lateral cartilage, the medial menisci are also significantly weakened (Fig. 6a). Since the direct biomechanical consequence of DMM is the meniscus-cartilage contact instability, meniscus can be affected by DMM more than other synovial tissues. The cartilage-meniscus misalignment created by DMM, coupled by OA-induced decrease in proteoglycan and alteration in interstitial fluid pressurization, will lead to extra wear on the meniscus. On the lateral side, while modulus reduction of cartilage is moderate but significant, such change in meniscus is marginal, which suggests that the degradation of meniscus likely lags that of condyle cartilage. Such difference can be due to both the lower concentration of proteoglycan, a more OA-susceptible constituent, in meniscus,[42] and the higher surface modulus of murine meniscus than cartilage.[24] By contrast, the subchondral bone and synovium do not exhibit substantial changes at 8 weeks post-surgery, conforming to the fact that DMM surgery has less direct impacts on these tissues than on cartilage and meniscus.

This study is the first to highlight meniscus mechanical changes in a murine PTOA model, contributing to a complete mechanical chronology of PTOA in multiple synovial tissues. As meniscus instability is a prevalent cause of PTOA,[2] our results further underscore the importance of examining and treating meniscus after injury.

4. Comparison to other nanomechanics studies of murine cartilage

This study is distinctive from previous nanomechanical studies of murine cartilage. Here, nanomechanical changes of cartilage are direct results of the DMM surgery, which has a well-defined OA progression timeline.[12] By contrast, previous studies mainly focused on the developmental defects in genetically modified cartilage. For instance, in collagen IX-null mice,[43] cartilage modulus decreases at 3-month age, earlier than the onset of spontaneous OA at one year age. However, such nanomechanical differences are developmental defects due to the loss of collagen IX, and are likely a major contributor, rather than the result, of OA. Similarly, in chondroadherin-null[19] and collagen VI-null[44] mice, the modulus reduction represents developmental defects, rather than OA symptoms.

On the other hand, our results of the Sham knee cartilage are in quantitative agreement with mature murine cartilage measured in other studies, which found an effective modulus ≈ 1–2MPa via both AFM-nanoindentation[19,43] and instrumented microindentation.[44,45] These values are higher than the modulus of murine growth plate cartilage recently measured on cross-sections (E_{ind} < 100kPa).[46] It is worth noting that murine cartilage has higher modulus

than larger species such as bovine,[47] porcine[48] and human,[43] which is attributed to the negative allometric scaling law.[32]

Cartilage exhibits salient rate-dependent mechanics, arising from both macromolecular friction-governed intrinsic viscoelasticity[49] and fluid flow-induced poroelasticity.[22] Recently, AFM-nanorheometric test showed that proteoglycan depletion results in >10-fold increase in murine cartilage hydraulic permeability, a deterministic factor of poroelasticity.[50] It is likely that besides modulus, other mechanical factors also undergo significant changes before the onset of PTOA. Our ongoing studies are using the custom AFM-nanorheometer[50] to probe into changes in the poroviscoelastic behaviors of cartilage after DMM. Nevertheless, as shown by this study, E_{ind} can adequately serve as a quantitative and sensitive indicator of PTOA (Fig. 7).

5. Conclusions

This study demonstrates the high sensitivity of nanoindentation modulus to the early stage degradation of cartilage in murine PTOA (Fig. 7). The decrease of modulus at 1–2 weeks after DMM can be due to the increased catabolic enzyme activities following the surgery. Blocking MMP and aggrecanase activities significantly attenuates this early modulus decrease. At the intermediate and late stage, progression of OA starts to influence the mechanics of lateral cartilage and medial meniscus. To our knowledge, this is the first study that quantifies the mechanical changes of articular cartilage and meniscus in a PTOA murine model. The results provide important knowledge for the pathomechanics of PTOA, as well as the search of early detection and prevention strategies. The methods presented here can be combined with genetically modified murine models to further elucidate the molecular etiology of PTOA.

Acknowledgments

This work was supported by the National Institutes of Health (Grants AR066824 to LH, AR060991, DK095803 to LQ, and AR050950), and the Department of Defense (W81XWH-13-1-0148 to XLL).

References

1. Olson, SA.; Guilak, F. Post-Traumatic Arthritis: Parthogenesis, Diagnosis and Management. New York, NY: Springer; 2015.
2. Lohmander LS, Englund PM, Dahl LL, Roos EM. The long-term consequence of anterior cruciate ligament and meniscus injuries: osteoarthritis. Am J Sports Med. 2007; 35:1756–1769. [PubMed: 17761605]
3. Yelin E, Callahan LF. The economic cost and social and psychological impact of musculoskeletal conditions. National Arthritis Data Work Groups. Arthritis Rheum. 1995; 38:1351–1362. [PubMed: 7575685]
4. Little CB, Zaki S. What constitutes an “animal model of osteoarthritis” - the need for consensus? Osteoarthr Cartilage. 2012; 20:261–267.
5. Lotz MK, Kraus VB. Posttraumatic osteoarthritis: pathogenesis and pharmacological treatment options. Arthritis Res Ther. 2010; 12:211. [PubMed: 20602810]
6. Anderson DD, Chubinskaya S, Guilak F, Martin JA, Oegema TR, Olson SA, et al. Post-traumatic osteoarthritis: improved understanding and opportunities for early intervention. J Orthop Res. 2011; 29:802–809. [PubMed: 21520254]

7. Fang H, Beier F. Mouse models of osteoarthritis: modelling risk factors and assessing outcomes. Nat Rev Rheumatol. 2014; 10:413–421. [PubMed: 24662645]
8. Little CB, Hunter DJ. Post-traumatic osteoarthritis: from mouse models to clinical trials. Nat Rev Rheumatol. 2013; 9:485–497. [PubMed: 23689231]
9. McNulty MA, Loeser RF, Davey C, Callahan MF, Ferguson CM, Carlson CS. Histopathology of naturally occurring and surgically induced osteoarthritis in mice. Osteoarthr Cartilage. 2012; 20:949–956.
10. Altman RD, Gold GE. Atlas of individual radiographic features in osteoarthritis, revised. Osteoarthr Cartilage. 2007; 15:A1–A56.
11. Hung CT, Ateshian GA. Grading of osteoarthritic cartilage: Correlations between histology and biomechanics. J Orthop Res. 2016; 34:8–9. [PubMed: 26694218]
12. Glasson SS, Blanchet TJ, Morris EA. The surgical destabilization of the medial meniscus (DMM) model of osteoarthritis in the 129/SvEv mouse. Osteoarthr Cartilage. 2007; 15:1061–1069.
13. Glasson SS, Askew R, Sheppard B, Carito B, Blanchet T, Ma HL, et al. Deletion of active ADAMTS5 prevents cartilage degradation in a murine model of osteoarthritis. Nature. 2005; 434:644–648. [PubMed: 15800624]
14. Jeon J, Oh H, Lee G, Ryu J-H, Rhee J, Kim J-H, et al. Cytokine-like 1 knock-out mice ($Cytl1^{-/-}$) show normal cartilage and bone development but exhibit augmented osteoarthritic cartilage destruction. J Biol Chem. 2011; 286:27206–27213. [PubMed: 21652695]
15. Sondergaard BC, Catala-Lehnen P, Huebner AK, Bay-Jensen AC, Schinke T, Henriksen K, et al. Mice over-expressing salmon calcitonin have strongly attenuated osteoarthritic histopathological changes after destabilization of the medial meniscus. Osteoarthr Cartilage. 2012; 20:136–143.
16. Zhang X, Zhu J, Liu F, Li Y, Chandra A, Levin LS, et al. Reduced EGFR signaling enhances cartilage destruction in a mouse osteoarthritis model. Bone Res. 2014; 2:14015. [PubMed: 26120493]
17. Miller RE, Tran PB, Ishihara S, Larkin J, Malfait AM. Therapeutic effects of an anti-ADAMTS-5 antibody on joint damage and mechanical allodynia in a murine model of osteoarthritis. Osteoarthr Cartilage. 2016; 24:299–306.
18. Ma HL, Blanchet TJ, Peluso D, Hopkins B, Morris EA, Glasson SS. Osteoarthritis severity is sex dependent in a surgical mouse model. Osteoarthr Cartilage. 2007; 15:695–700.
19. Batista MA, Nia HT, Önnerfjord P, Cox KA, Ortiz C, Grodzinsky AJ, et al. Nanomechanical phenotype of chondroadherin-null murine articular cartilage. Matrix Biol. 2014; 38:84–90. [PubMed: 24892719]
20. Buschmann MD, Kim Y-J, Wong M, Frank E, Hunziker EB, Grodzinsky AJ. Stimulation of aggrecan synthesis in cartilage explants by cyclic loading is localized to regions of high interstitial fluid flow. Arch Biochem Biophys. 1999; 366:1–7. [PubMed: 10334856]
21. Oliver WC, Pharr GM. An improved technique for determining hardness and elastic modulus using load and displacement sensing indentation experiments. J Mater Res. 1992; 7:1564–1583.
22. Mow VC, Kuei SC, Lai WM, Armstrong CG. Biphasic creep and stress relaxation of articular cartilage in compression: theory and experiments. J Biomech Eng. 1980; 102:73–84. [PubMed: 7382457]
23. Han, L.; Grodzinsky, AJ. Advances and applications of nanomechanical tools in cartilage tissue engineering. In: Zreiqat, H.; Dunstan, CR.; Rosen, V., editors. A Tissue Regeneration Approach to Bone and Cartilage Repair. Switzerland: Springer Int. Pub; 2015. p. 191-218.
24. Li Q, Doyran B, Gamer LW, Lu XL, Qin L, Ortiz C, et al. Biomechanical properties of murine meniscus surface via AFM-based nanoindentation. J Biomech. 2015; 48:1364–1370. [PubMed: 25817332]
25. Haywood L, McWilliams DF, Pearson CI, Gill SE, Ganesan A, Wilson D, et al. Inflammation and angiogenesis in osteoarthritis. Arthritis Rheum. 2003; 48:2173–2177. [PubMed: 12905470]
26. Flannery CR, Lark MW, Sandy JD. Identification of a stromelysin cleavage site within the interglobular domain of human aggrecan. Evidence for proteolysis at this site in vivo in human articular cartilage. J Biol Chem. 1992; 267:1008–1014. [PubMed: 1730630]

27. Zhang X, Zhu J, Liu F, Li Y, Chandra A, Levin LS, et al. Reduced EGFR signaling enhances cartilage destruction in a mouse osteoarthritis model. Bone Res. 2014; 2:14015. [PubMed: 26120493]
28. Fukui T, Tenborg E, Yik JH, Haudenschild DR. In-vitro and in-vivo imaging of MMP activity in cartilage and joint injury. Biochem Biophys Res Commun. 2015; 460:741–746. [PubMed: 25817731]
29. Nuti E, Santamaria S, Casalini F, Yamamoto K, Marinelli L, La Pietra V, et al. Arylsulfonamide inhibitors of aggrecanases as potential therapeutic agents for osteoarthritis: synthesis and biological evaluation. Eur J Med Chem. 2013; 62:379–394. [PubMed: 23376997]
30. Conover WJ, Iman RL. Rank transformations as a bridge between parametric and nonparametric statistics. Amer Statistician. 1981; 35:124–129.
31. Dimitriadis EK, Horkay F, Maresca J, Kachar B, Chadwick RS. Determination of elastic moduli of thin layers of soft material using the atomic force microscope. Biophys J. 2002; 82:2798–2810. [PubMed: 11964265]
32. Malda J, de Grauw JC, Benders KEM, Kik MJL, van de Lest CHA, Creemers LB, et al. Of mice, men and elephants: the relation between articular cartilage thickness and body mass. PLoS One. 2013; 8:e57683. [PubMed: 23437402]
33. Saarakkala S, Julkunen P, Kiviranta P, Mäkitalo J, Jurvelin JS, Korhonen RK. Depth-wise progression of osteoarthritis in human articular cartilage: investigation of composition, structure and biomechanics. Osteoarthr Cartilage. 2010; 18:73–81.
34. Ateshian GA. The role of interstitial fluid pressurization in articular cartilage lubrication. J Biomech. 2009; 42:1163–1176. [PubMed: 19464689]
35. Ruggiero L, Zimmerman BK, Park M, Han L, Wang L, Burris DL, et al. Roles of the fibrous superficial zone in the mechanical behavior of TMJ condylar cartilage. Ann Biomed Eng. 2015; 43:2652–2662. [PubMed: 25893511]
36. Caterson B, Flannery CR, Hughes CE, Little CB. Mechanisms involved in cartilage proteoglycan catabolism. Matrix Biol. 2000; 19:333–344. [PubMed: 10963994]
37. Iatridis JC, Godburn K, Wuertz K, Alini M, Roughley PJ. Region-dependent aggrecan degradation patterns in the rat intervertebral disc are affected by mechanical loading in vivo. Spine. 2011; 36:203–209. [PubMed: 20714280]
38. Bae WC, Temple MM, Amiel D, Coutts RD, Niederauer GG, Sah RL. Indentation testing of human cartilage: sensitivity to articular surface degeneration. Arthritis Rheum. 2003; 48:3382–3394. [PubMed: 14673990]
39. Waldstein W, Perino G, Gilbert SL, Maher SA, Windhager R, Boettner F. OARSI osteoarthritis cartilage histopathology assessment system: A biomechanical evaluation in the human knee. J Orthop Res. 2016; 34:135–140. [PubMed: 26250350]
40. Mow V, Guo XE. Mechano-electrochemical properties of articular cartilage: their inhomogeneities and anisotropies. Annu Rev Biomed Eng. 2002; 4:175–209. [PubMed: 12117756]
41. Temple-Wong MM, Bae WC, Chen MQ, Bugbee WD, Amiel D, Coutts RD, et al. Biomechanical, structural, and biochemical indices of degenerative and osteoarthritic deterioration of adult human articular cartilage of the femoral condyle. Osteoarthr Cartilage. 2009; 17:1469–1476.
42. Nakano T, Dodd CM, Scott PG. Glycosaminoglycans and proteoglycans from different zones of the porcine knee meniscus. J Orthop Res. 1997; 15:213–220. [PubMed: 9167623]
43. Stolz M, Gottardi R, Raiteri R, Miot S, Martin I, Imer R, et al. Early detection of aging cartilage and osteoarthritis in mice and patient samples using atomic force microscopy. Nat Nanotechnol. 2009; 4:186–192. [PubMed: 19265849]
44. Alexopoulos LG, Youn I, Bonaldo P, Guilak F. Developmental and osteoarthritic changes in Col6a1-knockout mice: biomechanics of type VI collagen in the cartilage pericellular matrix. Arthritis Rheum. 2009; 60:771–779. [PubMed: 19248115]
45. Cao L, Youn I, Guilak F, Setton LA. Compressive properties of mouse articular cartilage determined in a novel micro-indentation test method and biphasic finite element model. J Biomech Eng. 2006; 128:766–771. [PubMed: 16995764]

46. Prein C, Warmbold N, Farkas Z, Schieker M, Aszodi A, Clausen-Schaumann H. Structural and mechanical properties of the proliferative zone of the developing murine growth plate cartilage assessed by atomic force microscopy. Matrix Biol. 2016; 50:1–15. [PubMed: 26454027]

47. Han L, Frank EH, Greene JJ, Lee H-Y, Hung H-HK, Grodzinsky AJ, et al. Time-dependent nanomechanics of cartilage. Biophys J. 2011; 100:1846–1854. [PubMed: 21463599]

48. McLeod MA, Wilusz RE, Guilak F. Depth-dependent anisotropy of the micromechanical properties of the extracellular and pericellular matrices of articular cartilage evaluated via atomic force microscopy. J Biomech. 2013; 46:586–592. [PubMed: 23062866]

49. Mak AF. The apparent viscoelastic behavior of articular cartilage - the contributions from the intrinsic matrix viscoelasticity and interstitial fluid flows. J Biomech Eng. 1986; 108:123–130. [PubMed: 3724099]

50. Nia HT, Gauci SJ, Azadi M, Hung H-H, Frank E, Fosang AJ, et al. High-bandwidth AFM-based rheology is a sensitive indicator of early cartilage aggrecan degradation relevant to mouse models of osteoarthritis. J Biomech. 2015; 48:162–165. [PubMed: 25435386]

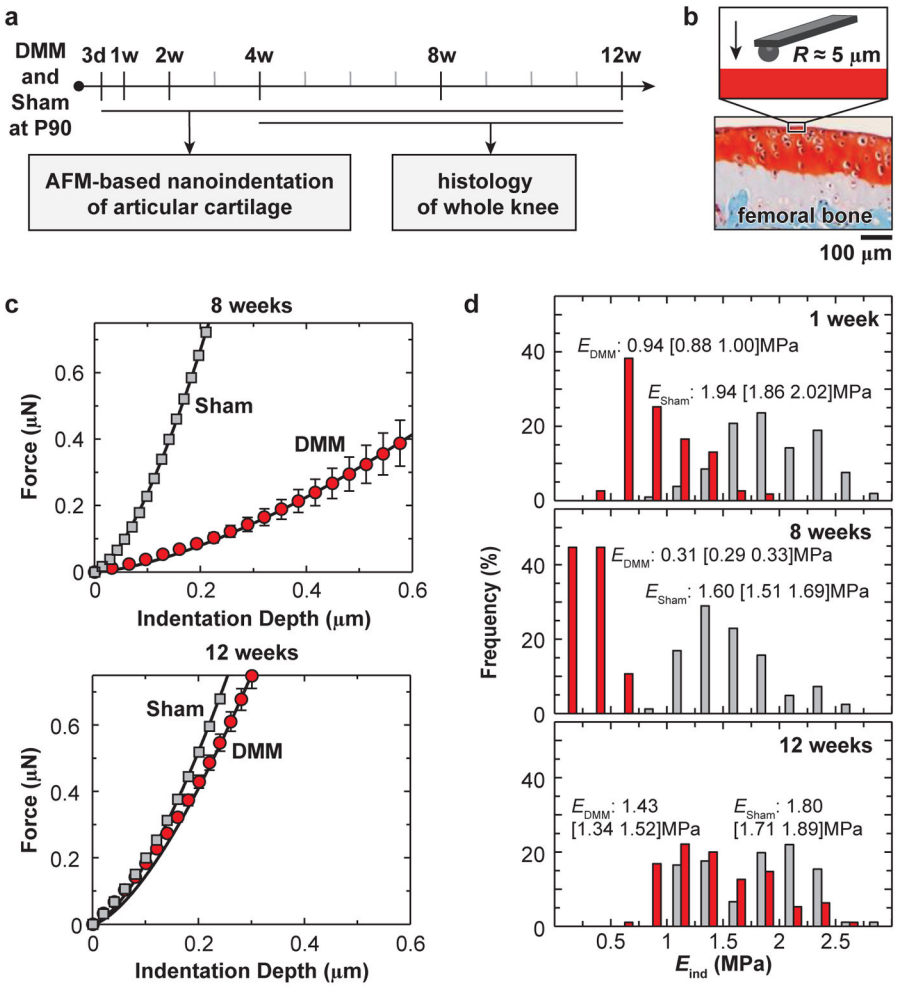

Fig. 1.

a) Experimental design and timeline of AFM-based nanoindentation and histology studies on murine knees after surgery-induced post-traumatic osteoarthritis. b) Schematic of nanoindentation on the femoral condyle cartilage via AFM-based nanoindentation. c) Typical indentation force, *F*, versus depth, *D*, curves on the medial condyle cartilage at 8 weeks and 12 weeks after the surgery (one mouse each time point), DMM on the right knee and Sham on the left knee, measured in PBS (tip radius $R \approx 5$ μm, 10 μm/s indentation depth rate, each error bar represents 95% confidence interval of ≥ 10 indentation locations, solid line: Hertz model fit of the mean *F-D* curve). d) Histograms of distribution of E_{ind} values obtained at all indentation locations (> 100 per group per time points) on all mice at 1 week, 8 weeks and 12 weeks after surgery. Kolmogorov-Smirnov test shows the data distribution is significantly different from normal distribution ($p < 0.001$).

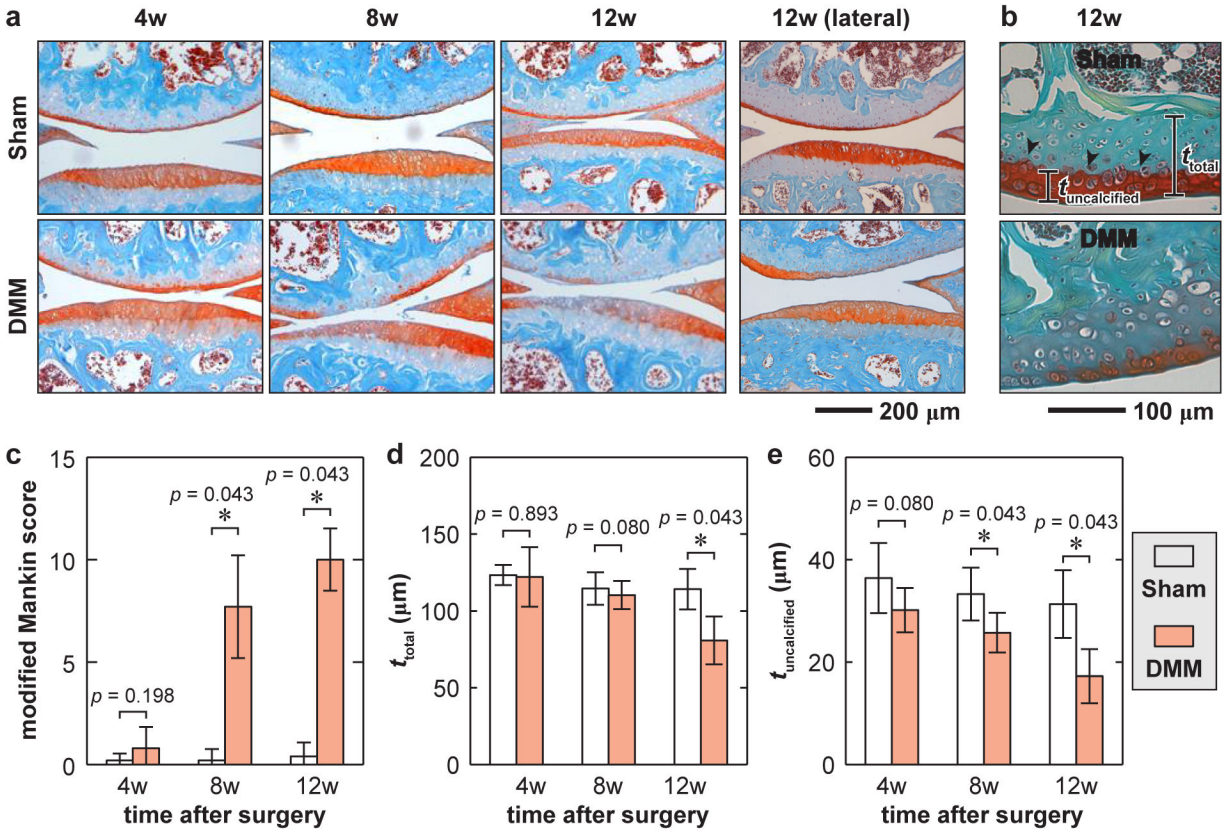

Fig. 2.

Histologic analysis illustrates OA progression of cartilage at 4 to 12 weeks after surgery. a) Representative Safranin-O/Fast Green-stained images showing cartilage thinning and reduced PG staining at 8 – 12 weeks post-surgery in the medial condyle of DMM knees, but not in Sham knees (Top bone: femur, bottom bone: tibia). Shown together are the histological images of lateral condyle at 12 weeks post-surgery. b) Definition of the total cartilage thickness, t_{total}, and uncalcified cartilage thickness, $t_{uncalcified}$, shown for 12 weeks after DMM. c) Modified Mankin score of DMM versus Sham knees. d–e) Comparisons of cartilage thickness. d) t_{total} and e) $t_{uncalcified}$ of DMM versus Sham knees at 4 – 12 weeks after surgery (each error bar represents 95% CI of condyles for the same surgery at the same time point, $n = 5$).

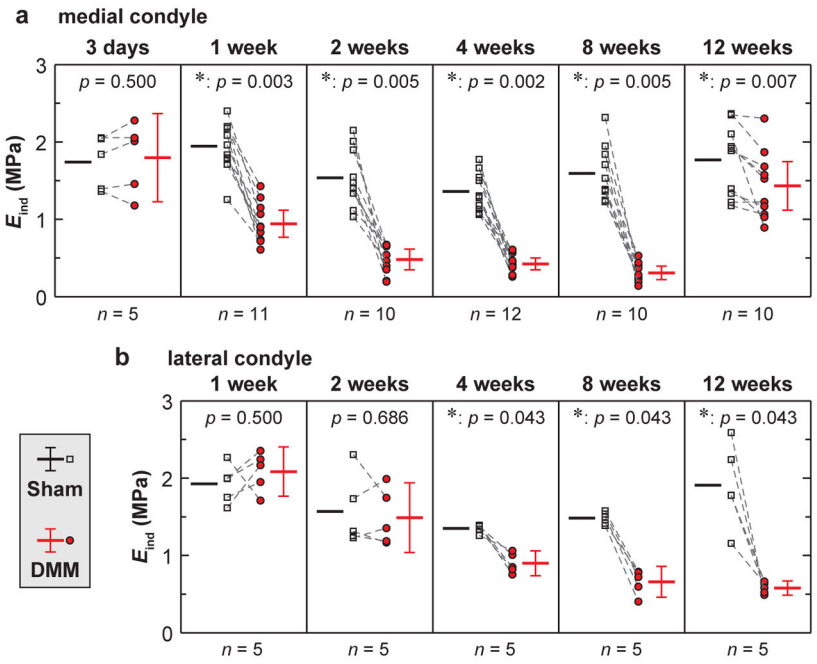

Fig. 3.

Effective nanoindentation modulus, E_{ind}, of condyle cartilage after surgery. a,b) Modulus, E_{ind}, of a) medial condyle cartilage at 3 days to 12 weeks after surgery, and b) lateral condyle cartilage at 1 to 12 weeks after surgery In panels a and b, each error bar represents 95% CI of the average E_{ind} from each condyle under the same surgery type and time point.

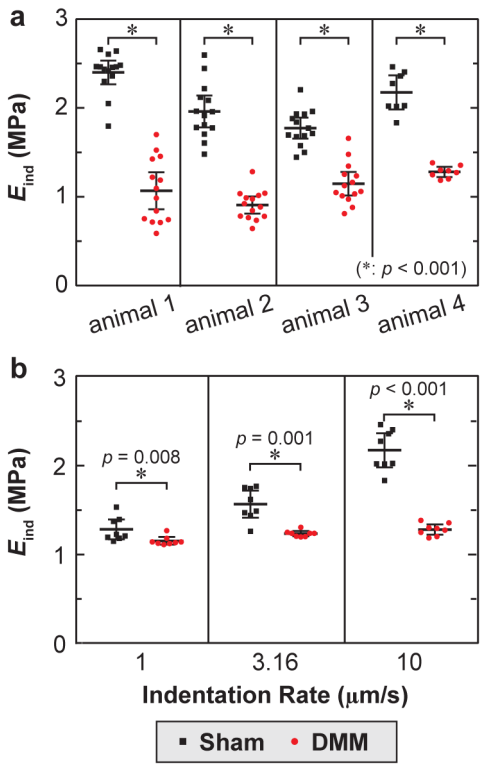

Fig. 4.

a) Significant reduction of E_{ind} on the DMM compared to the Sham knee cartilage within each individual animal at 1 week after surgery. b) Significant rate dependence of E_{ind} for cartilage after both DMM and Sham ($p < 0.001$ via repeated measure one-way analysis of variance on the global rank transforms of actual data, animal 4 in panel a). Each error bar represents 95% CI of ≥ 10 locations of cartilage on one murine medial condyle.

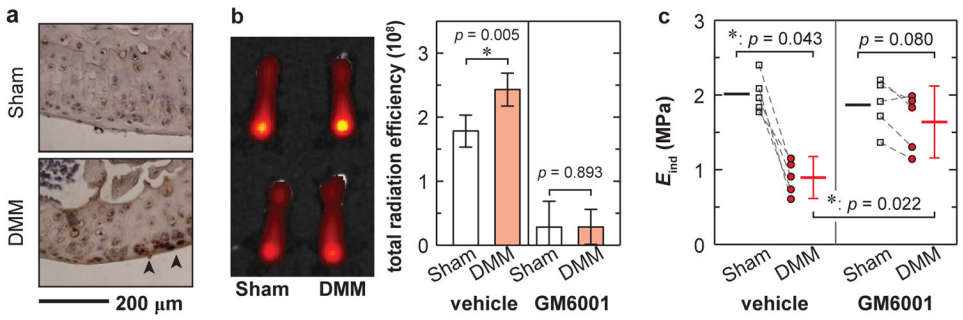

Fig. 5.

a) Immunohistochemical stains revealed an increase in the production of VDIPEN^{341}, the cleaved neoepitope of aggrecan by MMPs at 2 weeks after DMM. b) In vitro imaging of mouse femurs after MMPSense^{TM} 645 fast injection showed more elevated enzymatic activities on the DMM knee compared to the Sham knee in vehicle-treated group ($n = 5$, each error bar represents 95% CI), while such contrast was markedly reduced in GM6001-injected group ($n = 10$). c) After GM6001 injection, the medial condyle cartilage modulus of the DMM knee was markedly increased to a level similar to the Sham control ($n = 5$, each error bar represents 95% CI).

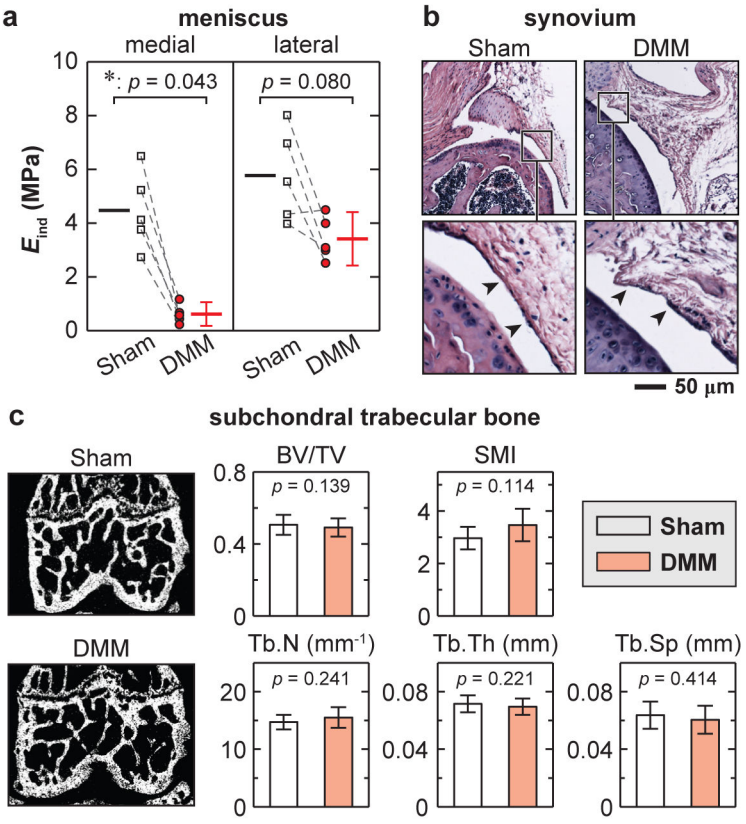

Fig. 6.

Osteoarthritic changes in meniscus, synovium and subchondral trabecular bone at 8 weeks after DMM surgery. a) Meniscus: AFM-based nanoindentation on meniscus surfaces illustrated marked modulus reduction on the medial side, and marginal changes on the lateral side after DMM ($n = 5$, each error bar represents 95% CI). b) Synovium: hematoxylin and eosin (H&E) staining showed no appreciable morphological differences ($n = 4$). c) Subchondral trabecular bone, left panel: frontal plane of µCT images, right panel: trabecular structural parameters calculated from µCT images ($n = 10$). Neither panel exhibited significant differences between DMM versus Sham knees.

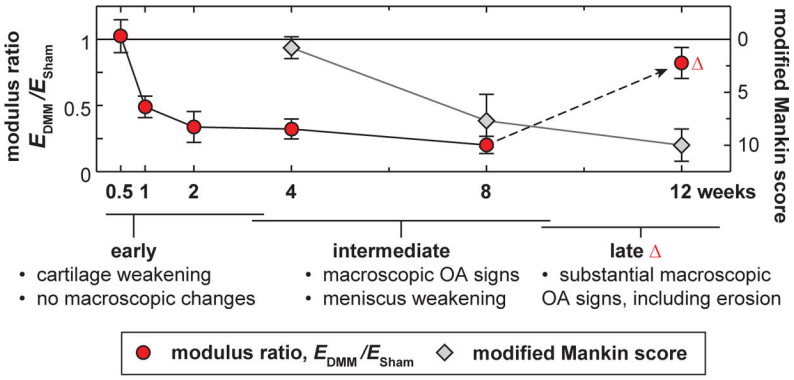

Fig. 7.

Comparison of timelines in the weakening of cartilage nanoindentation modulus (E_{DMM}/E_{Sham}) and histology-based modified Mankin scores in the DMM-induced OA murine model. The nanoindentation technique represents higher sensitivity to detect cartilage degradation compared to histology (each error bar represents 95% CI).